JAMES | Journal of Advances in Modeling Earth Systems

RESEARCH ARTICLE
10.1029/2019MS001693

Adaptive Localization for Satellite Radiance Observations in an Ensemble Kalman Filter

Lili Lei[1,2], Jeffrey S. Whitaker[3], Jeffrey L. Anderson[4], and Zhemin Tan[1,2]

[1]Key Laboratory of Mesoscale Severe Weather, Ministry of Education, Nanjing University, Nanjing, China, [2]School of Atmospheric Sciences, Nanjing University, Nanjing, China, [3]NOAA/Earth System Research Laboratory/Physical Sciences Division, Boulder, CO, USA, [4]National Center for Atmospheric Research, Boulder, CO, USA

Key Points:
- An adaptive method is proposed to estimate effective vertical localizations independently for each channel of every satellite platform
- Using adaptive localization width and vertical location for radiances is more beneficial than including the maximum localization value
- The adaptive localization parameters outperform the default GC and produce similar results to the optimal GC but with less computations

Correspondence to:
L. Lei,
lililei@nju.edu.cn

Citation:
Lei, L., Whitaker, J. S., Anderson, J. L., & Tan, Z. (2020). Adaptive localization for satellite radiance observations in an ensemble Kalman filter. *Journal of Advances in Modeling Earth Systems*, *12*, e2019MS001693. https://doi.org/10.1029/2019MS001693

Received 19 MAR 2019
Accepted 26 JUN 2020
Accepted article online 30 JUN 2020

Abstract Localization is essential to effectively assimilate satellite radiances in ensemble Kalman filters. However, the vertical location and separation from a model grid point variable for a radiance observation are not well defined, which results in complexities when localizing the impact of radiance observations. An adaptive method is proposed to estimate an effective vertical localization independently for each assimilated channel of every satellite platform. It uses sample correlations between ensemble priors of observations and state variables from a cycling data assimilation to estimate the localization function that minimizes the sampling error. The estimated localization functions are approximated by three localization parameters: the localization width, maximum value, and vertical location of the radiance observations. Adaptively estimated localization parameters are used in assimilation experiments with the National Centers for Environmental Prediction (NCEP) Global Forecast System (GFS) model and the National Oceanic and Atmospheric Administration (NOAA) operational ensemble Kalman filter (EnKF). Results show that using the adaptive localization width and vertical location for radiance observations is more beneficial than also including the maximum localization value. The experiment using the adaptively estimated localization width and vertical location performs better than the default Gaspari and Cohn (GC) experiment, and produces similar errors to the optimal GC experiment. The adaptive localization parameters can be computed during the assimilation procedure, so the computational cost needed to tune the optimal GC localization width is saved.

Plain Language Summary Assimilation of satellite radiance observations is essential for numerical weather predictions, especially where conventional observations are limited. Satellite radiances effectively measure integrated quantities over an atmospheric column, but it is not straightforward to d efine the vertical location of such a nonlocal observation. This results in complexities for localizing the impact of radiance observations; however, localization is crucial to effectively assimilate satellite radiances. This study investigated an adaptive localization approach to estimate an effective vertical localization independently for each assimilated channel of every satellite platform. Three localization parameters, including the localization width, maximum value, and vertical location of the radiance observations, were examined. It is demonstrated that using the adaptive localization width and vertical location for radiance observations is more beneficial than also including the maximum localization value. The adaptive localization method performs similarly to the optimal Gaspri and Cohn (GC) function, but the adaptive localization has significant computational cost advantages because it does not require intensive tuning of the localization width like the GC localization function.

1. Introduction

Satellite radiance observations have been assimilated by many operational numerical weather prediction (NWP) centers (e.g., Andersson et al., 1994; Derber & Wu, 1998; Kazumori, 2014). Radiance observations are essential for good forecast performance, especially where conventional observations are limited (Collard & McNally, 2009; Le Marshall, 2006; McCarty et al., 2009; McNally et al., 2006). Theoretically, direct radiance assimilation is superior to retrieval assimilation, since the retrieval process can introduce additional errors to the radiance observations. Unlike "conventional" observations (e.g., observations of model state variables like wind, temperature, and humidity), satellite radiances are nonlocal since they effectively measure integrated quantities over an atmospheric column. It is unclear how to define the location of such a

nonlocal observation; consequently, the vertical distances between a radiance observations and model state variables are not well defined (Lei et al., 2016; Lei & Whitaker, 2015).

The ensemble Kalman filter (EnKF; Burgers et al., 1998; Evensen, 1994) has been used to assimilate satellite radiances (Houtekamer et al., 2005). The EnKF uses an ensemble of forecasts to estimate the flow-dependent background error covariance, and it has been widely used in atmospheric applications (Aksoy et al., 2009; Buehner et al., 2010a, 2010b; Houtekamer et al., 2014; Snyder & Zhang, 2003; Tong & Xue, 2005; Whitaker et al., 2008). With high-dimensional atmospheric models, the EnKF is subject to sampling error that can lead to degraded analyses and filter divergence, because the affordable ensemble size ($\sim 10^2$) is much smaller than the dimension of the model's attractor. To combat sampling error, covariance localization is used to limit the impact of observations on remote state variables while preserving meaningful impacts on nearby state variables (Houtekamer & Mitchell, 1998).

For a serial EnKF that assimilates observations singly or in batches, covariance localization is often implemented by multiplying the sample covariance of an observation with a model state variable by a localization function (Hamill et al., 2001; Houtekamer & Mitchell, 2001). A commonly used localization function is the compactly supported polynomial approximation of a normal distribution given by Gaspari and Cohn (1999; GC). In the local ensemble transform Kalman filter (LETKF; Hunt et al., 2007; Miyoshi et al., 2007; Ott et al., 2004), localization is implicitly implemented by applying the assimilation algorithm on local regions with distance-dependent observation error variances. Rather than implementing localization in observation space like the EnKF and LETKF, some ensemble-variational data assimilation systems (Kleist & Ide, 2015; X. Wang et al., 2008) utilize localization in model space, by performing a Schur (Hadamard) product of the sample background error covariance matrix and a positive semidefinite localization matrix. Model space vertical localization can also be implemented in the EnKF and LETKF (Bishop et al., 2017; Lei et al., 2018), and the EnKF and LETKF with model space localization produce similar results to the four-dimensional ensemble-variational method (4DEnVAR) with full ensemble background error covariances (Lei et al., 2018). Localizing the impact of radiance observations in model space is usually superior to localizing in observation space (Campbell et al., 2010; Lei et al., 2018), but the opposite can be true when significant negative background error covariance occurs (Lei & Whitaker, 2015).

Radiance observations do not have a well-defined vertical location which poses challenges for effective observation space localization with an EnKF. Houtekamer et al. (2005) and Houtekamer and Mitchell (2005) treated the Advanced Microwave Sounding Unit-A (AMSU-A) radiance observations as local observations with vertical locations given by the level with maximum weighting function and then applied a GC localization function. However, the correlation between radiance observations and model state variables in a column can be very different from that between local observations and model state variables (Anderson & Lei, 2013). Previous studies also found that different localization functions are preferred for different observation types (Houtekamer & Mitchell, 2005; Lei et al., 2015; Lei & Anderson, 2014c), different kinds of state variables (Anderson, 2007, 2012; Kang et al., 2011), and different assimilation times (Anderson, 2007; Chen & Oliver, 2010). Thus, methods that compute the localization function adaptively have been investigated for the EnKF (Anderson, 2007, 2012; Bishop & Hodyss, 2009a, 2009b; Emerick & Reynolds, 2010; Lei & Anderson, 2014a, 2014b; Zhen & Zhang, 2014; Zhou et al., 2008).

Covariance localization is often divided into separate horizontal and vertical components (Houtekamer et al., 2005). Because satellite radiances provide information about temperature, moisture, and other trace gases in an atmospheric column, efforts have focused on improving estimates of the vertical localization functions for the radiances. Without assigning a vertical location to radiance observations, Lei et al. (2016) used a global group filter (GGF) to estimate vertical localization for AMSU-A radiance observations as a function of model pressure. Fertig et al. (2007) proposed in an LETKF to update the model state at a given location by radiance observations that are strongly correlated to the model state within a local region. Instead of using a single GC localization function for all satellite platforms and channels, Lei et al. (2016) used the GGF to compute independent vertical localization functions for every channel of AMSU-A. Miyoshi and Sato (2007) and Miyoshi et al. (2010) used the normalized sensitivity function based on the vertical differential of the transmittance as a vertical localization function for radiances from different satellite platforms.

Lei et al. (2016) demonstrated that the GGF can estimate a single vertical localization function for the AMSU-A radiance observations. They also examined the fitted GGF that approximates the GGF with a

GC localization for the AMSU-A radiance observations, and found that the GC fitted to the GGF produced slightly better forecasts than the GGF itself. Since it is not currently feasible to implement thousands of vertical localization functions for various types of radiance data due to the complexity of the vertical localization functions, the fitted GGFs are used here as vertical localization functions for each channel of every satellite being assimilated. Instead of using climatological sample correlations as in Lei et al. (2016), the fitted GGFs here use sample correlations between ensemble priors of observations and state variables from cycled assimilation in order to better estimate the sampling error in ensemble correlations. Moreover, to bypass the complexity of the adaptively estimated vertical localization functions and practically incorporate them in assimilating the radiance data, parameters that measure the properties of the estimated vertical localization functions and the impact of the parameters on the radiance data assimilation are investigated.

The remainder of this paper is organized as follows. The construction of fitted GGFs and the estimation of localization parameters are described in section 2. Section 3 presents the experimental design. The resulting fitted GGFs and associated localization parameters are discussed in section 4. Section 5 presents the assimilation results using the localization parameters extracted from the fitted GGFs. Section 6 summarizes the results.

2. Methodology

In an ensemble assimilation experiment, ensemble priors of observations and state variables are created for each assimilation cycle. For each assimilation cycle, define $\mathbf{Y}^o$ as the set of all ensemble prior estimates for one type of observation (e.g., National Oceanic and Atmospheric Administration (NOAA)-15 AMSU-A Channel 6 or MetOp-A IASI Channel 125). Let $y_{l,n}$ be an element of $\mathbf{Y}^o$, $l\in\{1, ..., L\}$ and $n\in\{1, ..., N\}$, where L is the total number of observations of this given type and N is the ensemble size. Define $\mathbf{X}^v$ as the set of all ensemble prior estimates for one class of state variable (e.g., temperature or humidity) that are interpolated to the horizontal locations of observations. An element of $\mathbf{X}^v$, $x^k_{l,n}$, $k\in\{1, ..., K\}$ where K is the number of model vertical levels, has the same horizontal location as $y_{l,n}$.

The sample correlations between the lth observation and the state variable interpolated to the horizontal location of this observation at vertical level k can be computed by $r^k_l=\frac{\sum_{n=1}^{N}\left(x^k_{l,n}-\overline{x^k_l}\right)\left(y_{l,n}-\overline{y_l}\right)}{\sqrt{\sum_{n=1}^{N}\left(x^k_{l,n}-\overline{x^k_l}\right)^2}\sqrt{\sum_{n=1}^{N}\left(y_{l,n}-\overline{y_l}\right)^2}}$, where $\overline{x^k_l}$ and $\overline{y_l}$ denote the ensemble mean of the state variable and observation respectively. The mean sample correlation at model level k for a given observation type and state variable kind is $\overline{r^k}=\frac{1}{L}\sum_{l=1}^{L}r^k_l$. The pressure at which the maximum of the absolute value of mean sample correlation occurs, denoted by p^o_v, is defined as the vertical location for the observation type paired with a state variable kind. Since the vertical location is estimated for an observation type, an individual observation no longer has a unique vertical location.

Lei and Anderson (2014a) and Lei et al. (2016) obtained the distribution of climatological correlation r by computing the correlation G times (also called G groups) through randomly drawn climatological perturbations. Here to achieve a distribution of the estimated sample correlation, the set of sample correlations r^k_l that relate with the same type of observation but at different horizontal locations is randomly partitioned into G mutually exclusive subsets of equal size, called groups. Denote the group sample correlations by $r^k_{m,g}$ $m\in\{1, ..., M\}$ and $g\in\{1, ..., G\}$, where M is the sample size for the groups. To better capture the distribution of the estimated sample correlation, a sufficiently large sample size M is needed for the G groups. Based on the distribution of the estimated sample correlations, the localization value α^k, that is, the adaptive vertical localization function (GGF), for a given observation type and state variable kind at model level k is defined to minimize the sampling error of the estimated sample correlations. Following Equation 2 in Lei and Anderson (2014a) and Equation 1 in Lei et al. (2016), α^k can be computed by

Table 1
List of Channels of Microwave Sounders Whose Localization Parameters Are Adaptively Estimated

Satellite	Sensor	Channels assimilated
NOAA-15	AMSU-A	1–10, 12–13, 15
NOAA-18	AMSU-A	1–8, 10–13, 15
	MHS	1–5
NOAA-19	AMSU-A	1–7, 9–13, 15
	MHS	1–5
AQUA	AMSU-A	6, 8–13
MetOp-A	AMSU-A	1–6, 8–13, 15
	MHS	1–5
MetOp-B	AMSU-A	1–13, 15
	MHS	1–5
SNPP	ATMS	1–14, 16–22

$$\alpha^k = \frac{\sum_{m=1}^{M}\left(\sum_{g=1}^{G} r_{m,g}^k\right)^2 / \sum_{m=1}^{M}\sum_{g=1}^{G}\left(r_{m,g}^k\right)^2 - 1}{G-1}. \quad (1)$$

The α^k minimizes the RMS difference of the estimated sample correlation from the other correlations in the same group for all M samples and G groups. Following Lei et al. (2016), the GGF is based on the distribution of the estimated correlations, since Anderson (2012) demonstrated that sampling error in the estimated regression coefficient is dominated by that in the estimated correlation. Also as shown by Equation 1, the GGF does not take into account the sequence of assimilation and correlations among observations.

To obtain a smoother localization function, the GC function is used to approximate the GGF; this is called fitted GC localization function (Lei et al., 2016). At 0 separation between an observation and a state variable, the GGF has estimated localization values between 0 and 1, while the GC function has a value of 1.0. Thus, multiplying the fitted GC with the GGF value at the vertical location p_v^o gives the scaled fitted GC localization function. Lei et al. (2016) showed that the fitted GC localization functions lead to slightly better forecasts than using the GGFs. Motivated by these results, the GC function, defined by an origin (location), width, and maximum value is used to fit the GGFs obtained here. Note that the fitted GC localization is a function of *ln* (pressure) like the GGF, thus using another vertical coordinate (e.g., scale height) might produce different fits. The GC width c_v^o is determined by the GC function that produces the smallest RMS difference compared to the GGF. The GC maximum $l\max_v^o$ is given by the GGF value at p_v^o and is between 0 and 1. Finally, the origin of the GC function is defined as the vertical location p_v^o.

Since satellite radiances are mostly sensitive to temperature and humidity, the three localization parameters are adaptively estimated for each channel of every satellite platform with state variable kind v being either temperature or specific humidity. A given channel and platform will be associated with a pair of vertical localization functions, one for temperature and one for specific humidity. The use of different localization functions by state variable kind and observation type may exacerbate the imbalance caused by data assimilation (Lei et al., 2015). Also, the estimated vertical locations of the observation p_v^o with different state variables can be inconsistent. Thus, the vertical localization function from the state variable that has the largest absolute value of mean sample correlation with one observation type (i.e., one channel of a satellite platform) is chosen, and the three adaptively estimated localization parameters from the chosen localization function are used for all state and observation updates in following ensemble assimilation experiments.

3. Experimental Design

The ensemble assimilation experiments use the National Centers for Environmental Prediction (NCEP) Global Forecast System (GFS) model with T254 resolution and 64 levels, a version of the 2016 operational GFS configuration, with a model top at 27 Pa. To clearly examine the impact of vertical localization on the assimilation of radiance observations, only radiance observations are assimilated in the ensemble assimilation experiments, except for the experiment that provides the bias correction for the satellite radiances. All radiance observations (http://www.emc.ncep.noaa.gov/mmb/data_processing/prepbufr.doc/table_18.htm) used in the NCEP Global Data Assimilation System (GDAS) are assimilated every 6 hr with a ±3-hr window. The channels of microwave sounders and infrared sounders whose localization parameters are adaptively estimated are listed in Tables 1 and 2, respectively.

The observation forward operator $\mathbf{H}$ and observation priors $\mathbf{H}\mathbf{x}^b$ (where $\mathbf{x}^b$ is the background or prior) for the ensemble mean and each ensemble member are computed by the Community Radiative Transfer Model (CRTM; Han et al., 2007; Weng, 2007) through the grid point statistical interpolation (GSI; Kleist et al., 2009; Wu et al., 2002) separately. The observation error variance $\mathbf{R}$ uses the same values as in the NCEP GDAS. The bias correction of satellite radiances is calculated from an experiment that assimilates both conventional (http://www.emc.ncep.noaa.gov/mmb/data_processing/prepbufr.doc/table_2.htm) and radiance

Table 2
List of Channels of Infrared Sounders Whose Localization Parameters Are Adaptively Estimated

Satellite	Sensor	Channels assimilated
AQUA	AIRS	21, 52, 72, 92, 93, 98–99, 104–105, 110, 116–117, 123, 128–129, 168–169, 172–174, 186, 190, 215–216, 221, 226–227
MetOp-A	HIRS/4	2–15
	IASI	16, 49, 51, 55, 57, 59, 61, 63, 66, 70, 72, 79, 81, 85, 87, 104, 106, 109, 111, 113, 116, 122, 125, 131, 135, 138, 146, 148, 151, 154, 157, 159, 161, 167, 170, 180, 185, 193, 199, 205, 230, 239, 254, 260, 262, 282, 296, 299
SNPP	CRIS	49, 51, 53, 59, 61, 63–65, 67, 69, 71, 73, 75, 79, 81, 83, 93, 101, 120, 123, 125
Meteosat-10	SEVIRI	2–3

observations that are used in the NCEP GDAS, using 4DEnVar (Kleist & Ide, 2015) with an 80-member ensemble and no static background error covariance component.

All ensemble assimilation experiments use an 80-member ensemble. The NOAA operational EnKF (http://www.dtcenter.org/com-GSI/users/docs/enkf_users_guide/EnKF_UserGuide_v1.0Beta.pdf) (an EnSRF) for the NCEP GFS is used. To maintain appropriate ensemble spread and avoid filter divergence, multiplicative covariance inflation that relaxes posterior ensemble spread back to prior ensemble spread (relaxation-to-prior spread; Whitaker & Hamill, 2012) is used, with the relaxation coefficient set to 0.85. Stochastic parameterizations (Palmer et al., 2009) are used to represent model uncertainty within the ensemble forecast step, and no additive inflation is applied. These assimilation parameters are adopted from the operational configuration. The four-dimensional incremental analysis update (4DIAU; Lei & Whitaker, 2016) is used to improve the balance of the analysis and better digest the observation information.

To mitigate spurious sample correlations due to limited ensemble size, localization is used. The localization is divided into separate horizontal and vertical components, and the product of these two components gives the final localization. For all experiments, horizontal localization uses the GC localization function with width 1,250 km. This horizontal localization scale is empirically chosen, but general results are expected to hold with a different horizontal localization scale, since radiance observations are integral observations in the vertical. For the vertical localization, experiment EnKF-GC*x* uses the GC localization function with a width of *x* (unit: *ln* (hPa)) whose default value is 1.5, the same as the value used in the operational GFS. Three additional experiments use different combinations of the estimated parameters from the GGFs. Details of the vertical localization used in the assimilation experiments are summarized in Table 3.

All experiments are run from 00 UTC 1 April 2014 to 00 UTC 15 April 2014. The GGFs are estimated based on the ensemble output from one assimilation cycle at 00 UTC 5 April 2014 from experiment EnKF-GC1.5. The group size G is set to 4, since Lei and Anderson (2014a) showed similar results with group sizes of 2 and 4. The first 4 days of assimilation are discarded to avoid transient effects, and the remaining data between 00 UTC 5 April 2014 and 00 UTC 15 April 2014 is used for verification. The evaluation is done in observation space using the 6-hr prior. The globally and temporally averaged root-mean-square (RMS) observation increment profiles of temperature, vector wind ($[(\mathbf{u}^o - \mathbf{u}^f)^2+(\mathbf{v}^o - \mathbf{v}^f)^2]/2$), and normalized specific humidity (specific humidity divided by saturation specific humidity) are verified relative to the conventional observations that include marine and land surface stations, rawinsonde, and aircraft.

Table 3
List of Experiments and Vertical Localization Used in the Assimilation Experiments

Exp. name	c_v^o	$l\max_v^o$	p_v^o
EnKF-GC*x*	*x*	1.0	pressure at the maximum weighting function
EnKF-GGFa	fitted GC from GGF	1.0	pressure at the maximum weighting function
EnKF-GGFb	fitted GC from GGF	1.0	from GGF
EnKF-GGFc	fitted GC from GGF	scaled fitted GC from GGF	from GGF

Note. The c_v^o (unit: *ln* (hPa)) is the width of GC localization function, $l\max_v^o$ is the maximum of fitted GC localization value, and p_v^o is vertical location of a given observation type.

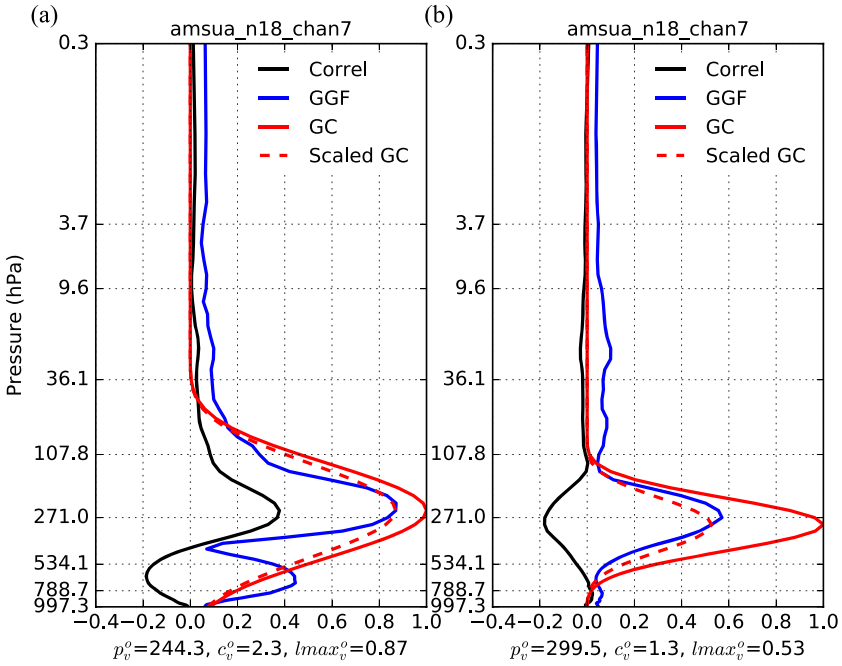

Figure 1. The mean correlation (black), estimated localization function GGF (blue), fitted GC localization function to the GGF (red solid), and scaled fitted GC localization function (red dashed) for state variables (a) temperature and (b) specific humidity of NOAA-18 AMSU-A Channel 7. The estimated three localization parameters p_v^o, c_v^o, and $l\max_v^o$ are denoted at the bottom.

4. Adaptive Localization Parameters

Localization parameters for assimilated radiance observations (Tables 1 and 2) are adaptively estimated by the method described in section 2. Taking NOAA-18 AMSU-A Channel 7 as an example, its mean correlation, estimated localization function GGF (scaled) fitted GC localization function to the GGF for state variables temperature and specific humidity are shown in Figure 1. The mean correlation of this type of radiance observation with state variable temperature changes from negative to positive in the vertical and has two maxima, while the mean correlation with state variable specific humidity is mainly negative and has one maximum. The maximum of the mean correlation with temperature is larger than that with specific humidity, and thus, the vertical location p_v^o of NOAA-18 AMSU-A Channel 7 radiance observation is 244.3 hPa, at which the mean correlation with temperature is maximum.

The GGFs estimated from the mean correlations with state variables temperature and specific humidity have similar shape to the absolute values of the mean correlations. This is because the signal-to-noise ratio increases with the absolute correlation value (Lei & Anderson, 2014a). Therefore, the GGF can provide an adaptive estimate of the localization function. To eliminate the possible impacts of imbalance caused by a nonsmooth localization function on subsequent model forecasts (Lei et al., 2016), the GC localization function is used to fit the GGF. The red solid lines in Figure 1 show the fitted GC functions; the localization widths c_v^o are 2.3 and 1.3 (unit: *ln* (hPa)) for state variables temperature and specific humidity respectively. The red dashed lines in Figure 1 show the scaled GC functions which are the fitted GC functions multiplied by the GGF value ($l\max_v^o$) at the observation vertical location p_v^o. The $l\max_v^o$ is 0.87 for the GGF with state variable temperature and 0.53 for the GGF with state variable specific humidity. Since the maximum of the mean correlation with temperature is larger than that with specific humidity, the fitted GC localization function width c_v^o and the maximum localization value $l\max_v^o$ estimated from the mean correlation with temperature are used for NOAA-18 AMSU-A Channel 7 in EnKF-GGF experiments.

The AMSU-A radiances are more sensitive to temperature than to specific humidity, but the Microwave Humidity Sounder (MHS) radiances are the opposite. Figure 2 shows the mean correlation, estimated localization function GGF, and (scaled) fitted GC localization function for state variables temperature and

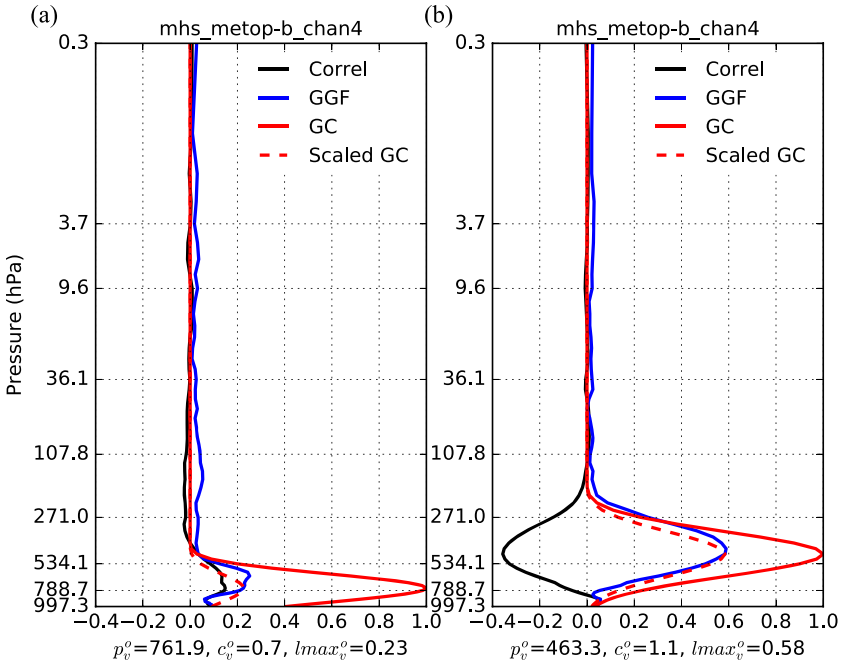

Figure 2. Same as Figure 1, except for of MetOp-B MHS Channel 4.

specific humidity for MetOp-B MHS Channel 4. The mean correlation of this type of radiance observation with state variable specific humidity has a maximum of 0.37, while the absolute value of the mean correlation with state variable temperature is less than 0.2. Thus, the three estimated localization parameters are chosen from the GGF and (scaled) fitted GC localization function for state variable specific humidity. The observation vertical location p_v^o, the fitted GC localization width c_v^o, and the maximum localization value $l\max_v^o$ are 463.3 hPa, 1.1 (unit: *ln* (hPa)) and 0.58. All three estimated localization parameters are larger than those estimated for the mean correlation and GGF with state variable temperature.

Figure 1a is very similar to Figure 4d in Lei et al. (2016), except that the maxima of the mean correlation and GGF localization function are smaller in Figure 1a than in Figure 4d, especially for the GGF localization values associated with the negative mean correlations. This may be because Lei et al. (2016) combined AMSU-A radiance observations from all satellite platforms (NOAA-15, NOAA-18, NOAA-19, AQUA, MetOP-A, and MetOP-B), but here only the NOAA-15 AMSU-A radiance observations are estimated. Also, Lei et al. (2016) estimated the sample correlation and GGF localization function using climatological ensemble perturbations, but here the sample correlation and GGF are computed from the cycled assimilation. The overall consistency between Figure 1a here and Figure 4d in Lei et al. (2016) demonstrates the ability of the GGF method, as an extension of the GGF used in Lei et al. (2016), to adaptively estimate the localization parameters for each channel from every satellite platform.

The mean and one standard deviation of the three estimated localization parameters over the six satellite platforms (Table 1) for the AMSU-A radiance observations are shown in Figure 3. Channel 14 is sensitive to conditions above the model top, so it is not assimilated. For Channels 4–13 that are not sensitive to surface conditions, the estimated observation vertical location moves upward from Channel 4 to Channel 13. The estimated p_v^o has small standard deviation among the satellite platforms, except for Channels 3 and 15. The fitted GC localization widths c_v^o and maximum localization values $l\max_v^o$ vary among the channels (Figures 3b and 3c). The mean values of c_v^o are generally consistent with the estimates in Table 1 of Lei et al. (2016). Channels that are not sensitive to surface conditions have c_v^o larger than the default value of GC localization width (1.5 *ln* (hPa)) shown by the dashed line, except for Channel 6. Channels that are sensitive to surface conditions (Channels 1–3 and 15) have c_v^o smaller than the default value of GC localization width, except for Channel 3. The estimated c_v^o from different satellite platforms generally agree with each

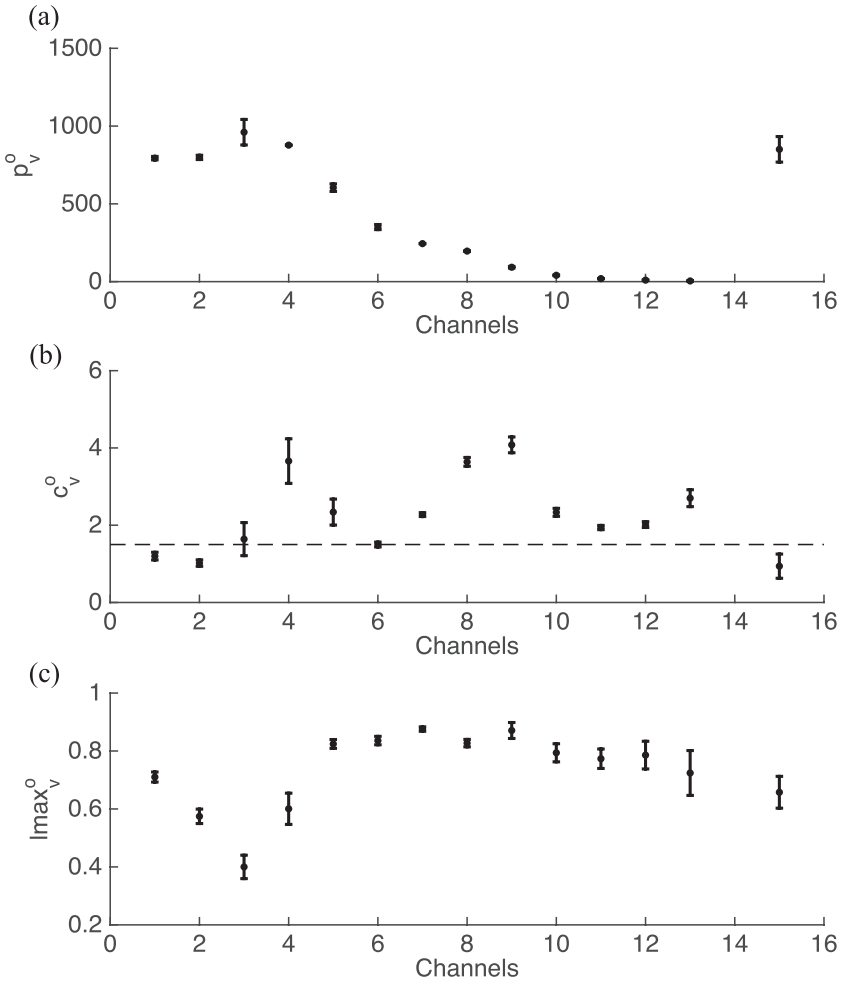

Figure 3. The mean and one standard deviation of the six satellite platform estimates of (a) the observation vertical location p_v^o, (b) the fitted GC localization width c_v^o, and (c) the maximum localization value $l\max_v^o$ for the AMSU-A radiance observations. The dashed line in (b) denotes the default GC localization width.

other, except that Channels 3–5 and 15 have larger standard deviation. The maximum localization value $l\max_v^o$ has mean value around 0.7–0.8 for most channels, while $l\max_v^o$ for Channels 2–4 are less than 0.6. There is a larger standard deviation of $l\max_v^o$ among satellite platforms for Channels 3–4, 12–13, and 15.

Figure 4 presents the mean and one standard deviation of the three estimated localization parameters for the MHS radiance observations from all four satellite platforms (Table 1). On average the estimated width c_v^o for MHS radiance observations is smaller than that for AMSU-A radiance observations. The estimated widths c_v^o for Channels 3–5 are larger than those for Channels 1–2, due to the different characteristics of the mean correlations. The mean correlations of MHS Channels 1–2 radiance observations with state variables temperature and specific humidity are dominated by positive values at low levels (figures not shown). The mean correlations of MHS Channels 3–5 radiance observations with state variable specific humidity is mainly negative while the correlation is mainly positive for temperature, and the mean correlation with state variable specific humidity has larger absolute value than that with state variable temperature (figures not shown). The maximum localization value $l\max_v^o$ decreases from Channel 3 to Channel 5, because the maximum mean correlation decreases from Channel 3 to Channel 5. The standard deviation of the estimated observation vertical location and fitted GC localization width among satellite platforms is larger for Channel 1 than for the other channels. This is because the three localization parameters for NOAA-18 are chosen from the GGF with state variable temperature, because the maximum of the mean correlation with state variables temperature and specific humidity are similar to each other for Channel 1. However, the three

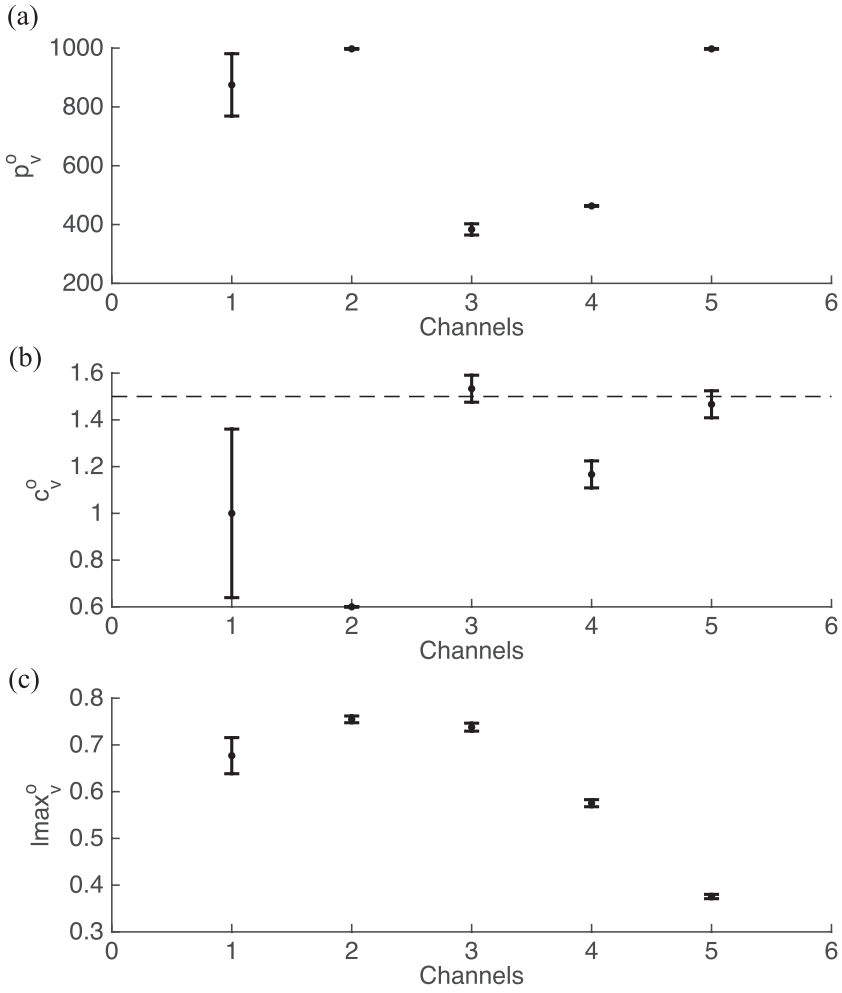

Figure 4. Same as Figure 3, except for the MHS radiance observations.

localization parameters for the other satellite platforms are chosen from the GGF with state variable specific humidity.

As an example of infrared sounders, the three estimated localization parameters for HIRS/4 onboard the MetOp-A satellite are shown in Figure 5. Channel 1 and Channels 16–19 of HIRS/4 onboard MetOp-A are not operationally used. For Channels 2–4, the estimated localization width c_v^o is larger than the default GC localization width because the observation vertical location is high (above 250 hPa) and the mean correlation with state variable temperature dominates and has a wide range (figures not shown). For Channels 5–15, the estimated localization width c_v^o is similar to or smaller than the default GC localization width. Although the observation vertical locations for Channels 11–12 are higher than 500 hPa, the mean correlations are dominated by those with state variable specific humidity, and thus, the estimated localization widths are close to the default GC localization width. The other channels between 5 and 15 are more sensitive to temperature, and given the low observation vertical location, the estimated localization widths are smaller than the default GC localization width. The maximum localization value $lmax_v^o$ is between 0.6 and 0.8 for most channels, except for Channels 8–10.

Therefore, the results from the infrared sounder HIRS/4 onboard MetOp-A are consistent with those from microwave sounders AMSU-A and MHS. The estimated localization parameters for the other infrared sounders listed in Table 2 are not shown, but similar results to HIRS/4 are obtained.

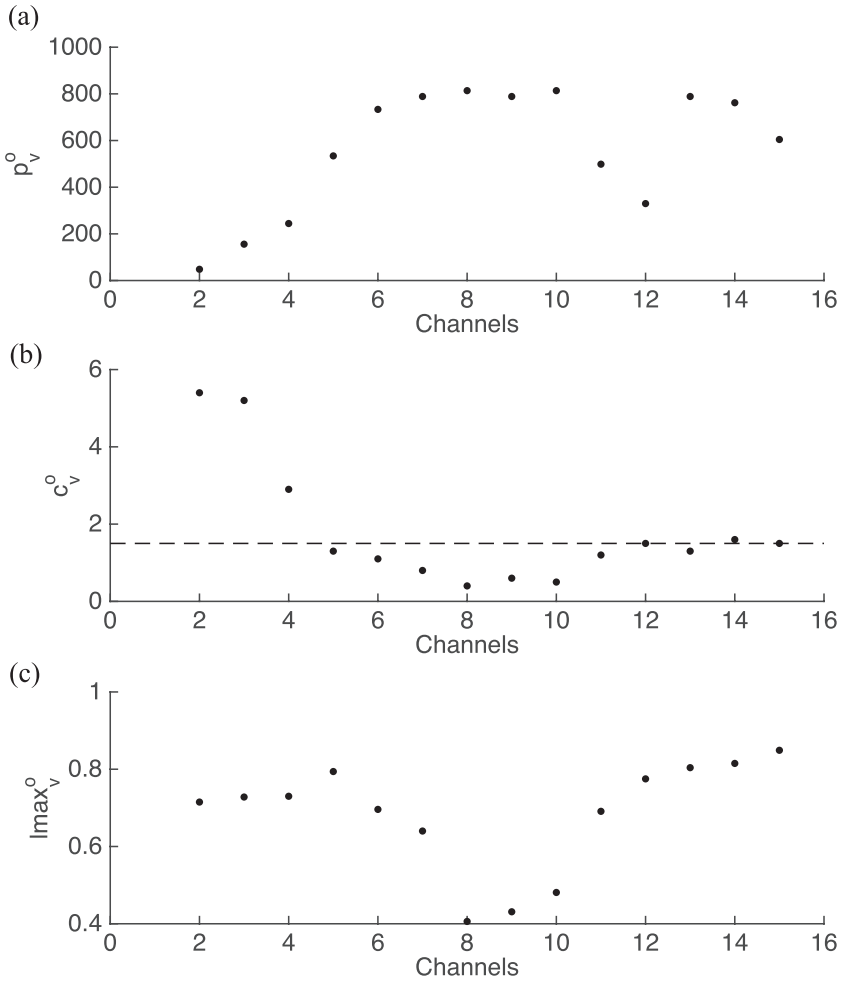

Figure 5. The value of (a) the observation vertical location p_v^o, (b) the fitted GC localization width c_v^o, and (c) the maximum localization value $lmax_v^o$ for the MetOp-A HIRS/4 radiance observations.

5. Assimilation Results

Besides experiment EnKF-GC1.5 that uses the default GC localization width (1.5 *ln* (hPa)), three assimilation experiments are conducted with different combinations of the three adaptively estimated localization parameters. As shown in Table 3, experiment EnKF-GGFa uses the estimated localization width c_v^o for each channel from every instrument onboard each satellite. Experiment EnKF-GGFb uses both c_v^o and the estimated vertical location p_v^o. Experiment EnKF-GGFc uses all three estimated localization parameters.

The globally and temporally averaged RMS observation increment profiles for the four experiments are shown in Figure 6. Please note that the RMS error differences among the experiments are more prominent in the Northern Hemisphere than in the Southern Hemisphere and Tropics, which is consistent with Lei et al. (2016); thus, only the globally averaged RMS errors are presented. Since experiment EnKF-GGFb generally has the smallest errors as shown below, the significance of the difference between experiment EnKF-GGFb and the other experiments is examined. One sample *t* tests are performed for the error samples of experiment EnKF-GGFb at each assimilation cycle and the mean errors of the other experiments. The error differences that are significant at the 95% confidence level are shown by the dots in Figure 6. Compared to experiment EnKF-GC1.5, experiment EnKF-GGFa reduces wind errors, especially between 600 and 100 hPa. Experiment EnKF-GGFa produces slightly smaller errors of temperature and normalized specific humidity than experiment EnKF-GC1.5. The improvements of experiment EnKF-GGFa compared to experiment EnKF-GC1.5 (Figure 6) are smaller than those obtained in Lei et al. (2016, their Figure 5).

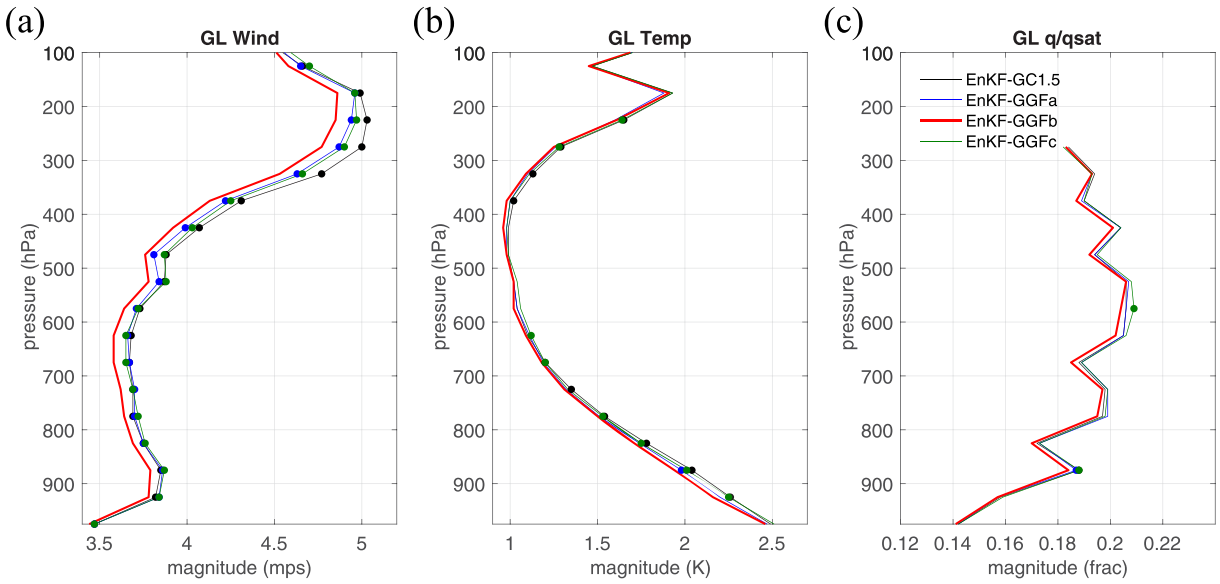

Figure 6. Globally and temporally averaged RMS observation increments for (a) vector wind, (b) temperature, and (c) normalized specific humidity (specific humidity divided by saturation specific humidity) for all conventional observations from Experiments EnKF-GC1.5, EnKF-GGFa, EnKF-GGFb, and EnKF-GGFc. The dots denote cases for which the difference between the experiment EnKF-GGFb and the compared experiment is significant at the 95% confidence level (using one sample *t* test).

This may be because Lei et al. (2016) assimilated only AMSU-A radiance observations but many more radiance observations are assimilated here. And also the imbalance caused by applying different localization widths for various radiance observation types (Lei et al., 2015) may have an impact on the application of GGF.

When the estimated observation vertical location p_v^o is included (experiment EnKF-GGFb), the wind errors are significantly reduced for all vertical levels and the temperature errors are significantly reduced below 700 hPa and between 200 and 400 hPa, compared to experiments EnKF-GC1.5 and EnKF-GGFa. The errors of normalized specific humidity are slightly decreased, but differences are only significant at 875 hPa. Therefore, applying the estimated localization width c_v^o has some advantages over the default GC localization width for assimilation of radiance observations. Applying both the estimated observation vertical location p_v^o and localization width c_v^o further increases the advantages over the default GC localization width.

However, when the maximum localization value $l\max_v^o$ is also used (experiment EnKF-GGFc), slightly larger errors than experiment EnKF-GGFa and slightly smaller errors than experiment EnKF-GC1.5 are obtained. Thus, applying the maximum localization value $l\max_v^o$ decreases the advantages of applying the estimated c_v^o and p_v^o over the default GC localization width. As shown in Figures 1–5, all estimated maximum localization values are less than 1.0, which is consistent with the estimated localization functions for spatially averaged observations in Anderson (2007). Since the maximum localization values are less than 1.0, the state variable increments given each radiance observation in experiment EnKF-GGFc are smaller than those in experiments EnKF-GGFa and EnKF-GGFb. This may indicate insufficient ensemble spread during assimilation cycles. Since the same parameters of multiplicative inflation and stochastic physics as the GC experiments are used for the GGF experiments, the performance of experiment EnKF-GGFc could be improved with optimally tuned inflation parameters. The reasons that including the maximum localization value degrades the performance of experiment EnKF-GGFc will be investaged in further studies.

Lei et al. (2016) showed that a broad GC localization width is preferred when assimilating the AMSU-A radiance observations, so sensitivity experiments that vary the value of GC localization width are conducted. The errors, especially the temperature errors, are reduced when the GC localization width increases from 1.5 to 3.0, but the errors are not further reduced when GC localization width is further increased (figures not shown). The globally and temporally averaged RMS observation increment profiles for experiment EnKF-GGFb and EnKF-GC3.0 that is the optimal GC width are shown in Figure 7. Compared to

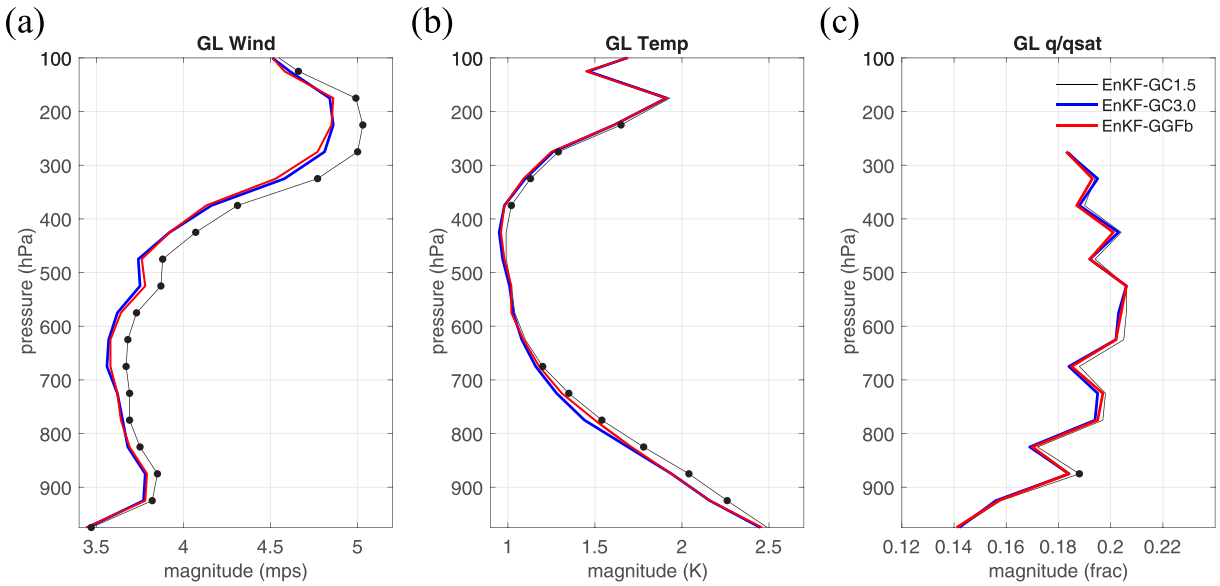

Figure 7. Same as Figure 6, except for experiments EnKF-GGFb, EnKF-GC1.5, and EnKF-GC3.0.

experiment EnKF-GC3.0, experiment EnKF-GGFb slightly reduces wind errors around 300 hPa but slightly increases wind errors around 500 hPa, and experiment EnKF-GGFb slightly decreases errors of normalized specific humidity around 400 hPa but slightly increases temperature errors around 800 hPa. However, these differences are not significant; thus, in general, experiments GGFb and EnKF-GC3.0 produce similar results to each other.

Experiment EnKF-GGFb does not outperform experiment EnKF-GC3.0 as in Lei et al. (2016), which is consistent with the previously noted result that the improvements of experiment EnKF-GGFa compared to experiment EnKF-GC1.5 are smaller than those in Lei et al. (2016). One possible reason is that the estimated localization width c_v^o varies among the channels of different sounders onboard multiple satellites, and the application of various localization widths results in imbalance compared to a single localization width, which reduces the advantages of applying adaptively estimated localization parameters. One advantage of EnKF-GGFb over EnKF-GC3.0 is that the three localization parameters can be computed along with the assimilation procedure and no additional computational cost is required, but tuning the GC localization width requires significant computation.

6. Conclusion

Vertical localization for radiance observations in observation space is not straightforward because the concepts of vertical location and separation are not well defined for the nonlocal radiance data. An adaptive method (GGF) is applied here to estimate the vertical localization for each channel and every satellite platform of radiance data. The GGF uses sample correlations between ensemble priors of observations and state variables from assimilation cycles to provide an estimate of the localization function that minimizes the sampling error of the estimated correlations. To obtain a smooth localization function, the fitted GGF is computed using the GC localization function to fit the GGF. Based on the fitted GGF, three localization parameters, the localization width, localization maximum, and vertical location of the radiance observations, are provided and used in assimilation experiments.

Results show that the GGF can provide adaptively estimated vertical localization functions for both microwave and infrared sounders. The adaptively estimated GGF localization function have similar shapes to the absolute value of the mean sample correlations. Unlike the GC localization function, the GGF localization function can have local maxima when significant correlations are present. The vertical localization function GGF for NOAA-18 AMSU-A Channel 7 with state variable temperature is similar to that obtained in Lei et al. (2016).

Based on the GGFs, the three localization parameters are adaptively obtained for each channel of every satellite being assimilated. For the AMSU-A radiances that are more sensitive to temperature than to specific humidity, the localization parameters are primarily obtained from the GGF with state variable temperature. Similarly, the localization parameters for the MHS radiances are primarily obtained from the GGF with state variable specific humidity. The vertical locations of radiance data vary with channels, but generally have only small differences among the satellite platforms for a given channel. The adaptively estimated localization widths and maximum localization values vary with satellite channels and platforms, which indicates the complexity and large computational cost to comprehensively tune the localization for radiance data empirically. The adaptively estimated maximum localization value is often smaller than 1.0.

These adaptively estimated localization parameters are used in assimilation experiments with the NCEP GFS and the NOAA operational EnKF. Experiments using the adaptively estimated localization parameters produce smaller 6-hr prior errors than the control experiment that uses the GC function with a default localization width (1.5 *ln* (hPa)). Similar results might occur for long forecast lead times. For instance, Lei et al. (2016) showed that the advantages of a related GGF application persisted through 120-hr forecast lead time in a global model. Examining the impacts for longer lead forecasts for the problems studied here should receive further study but is beyond the scope of this report. Results show that using the adaptive localization width and vertical location of radiance observations is more beneficial than including the maximum localization value. The experiment using the adaptively estimated localization width and vertical location produces very similar errors to the optimal GC experiment. However, the adaptive localization parameters can be computed as part of the assimilation procedure, so the computational cost needed to tune the optimal GC localization width is saved.

The adaptive localization method applied to each assimilated channel of every satellite platform and the key localization parameters has been demonstrated here. Spatial and temporal variations of the adaptive localization parameters are investigated in a separate study (C. Wang et al., 2020), which shows the benefits of spatially and temporally varying localization parameters for tropical cyclone assimilations and forecasts. The imbalance in subsequent model forecasts caused by applying different localization scales with various channels and satellite platforms needs further investigation. The adaptive localization algorithm could improve the representation of cloud when it is applied for all-sky radiance data assimilation. These potential improvement and usage of the adaptive localization algorithm will be presented in future studies.

Data Availability Statement

The data used to generate the simulation experiments were obtained from the National Centers for Environmental Prediction (NCEP; https://www.ncdc.noaa.gov/data-access/model-data/model-datasets/global-forcast-system-gfs). The globally and temporally averaged 6-hr RMS observation increments from each experiment are available online (https://meso.nju.edu.cn/xwdt/20200525/i101472.html).

Acknowledgments

This work is supported by the National Key Research and Development Program of China under Grant 2017YFC1501603 and the General Program of National Natural Science Foundation of China under Grants 41922036 and 41675052. The National Center for Atmospheric Research is sponsored by the National Science Foundation. Any opinions, findings, and conclusions or recommendations expressed in this publication are those of the authors and do not necessarily reflect the views of the National Science Foundation.

References

Aksoy, A., Dowell, D. C., & Snyder, C. (2009). A multicase comparative assessment of the ensemble Kalman filter for assimilation of radar observations. Part I: Storm-scale analyses. *Monthly Weather Review*, *137*(6), 1805–1824. https://doi.org/10.1175/2008MWR2691.1

Anderson, J. L. (2007). Exploring the need for localization in ensemble data assimilation using a hierarchical ensemble filter. *Physica D*, *230*(1-2), 99–111. https://doi.org/10.1016/j.physd.2006.02.011

Anderson, J. L. (2012). Localization and sampling error correction in ensemble Kalman filter data assimilation. *Monthly Weather Review*, *140*(7), 2359–2371. https://doi.org/10.1175/MWR-D-11-00013.1

Anderson, J. L., & Lei, L. (2013). Empirical localization of observation impact in ensemble Kalman filters. *Monthly Weather Review*, *141*(11), 4140–4153. https://doi.org/10.1175/MWR-D-12-00330.1

Andersson, E., Pailleux, J., Thepaut, J.-N., Eyre, J. R., McNally, A. P., Kelly, G. A., & Courtier, P. (1994). Use of cloud-cleared radiances in three/four-dimensional variational data assimilation. *Quarterly Journal of the Royal Meteorological Society*, *120*(517), 627–653. https://doi.org/10.1002/qj.49712051707

Bishop, C. H., & Hodyss, D. (2009a). Ensemble covariances adaptively localized with ECO-RAP. Part 1: Tests on simple error models. *Tellus*, *61A*, 84–96.

Bishop, C. H., & Hodyss, D. (2009b). Ensemble covariances adaptively localized with ECO-RAP. Part 2: Astrategy for the atmosphere. *Tellus*, *61A*, 97–111.

Bishop, C. H., Whitaker, J. S., & Lei, L. (2017). Gain form of the ensemble transform Kalman filter and its relevance to satellite data assimilation with model space ensemble covariance localization. *Monthly Weather Review*, *145*(11), 4575–4592. https://doi.org/10.1175/MWR-D-17-0102.1

Buehner, M., Houtekamer, P. L., Charette, C., Mitchell, H. L., & He, B. (2010a). Intercomparison of variational data assimilation and the ensemble Kalman filter for global deterministic NWP. Part I: Description and single-observation experiments. *Monthly Weather Review*, *138*(5), 1550–1566. https://doi.org/10.1175/2009MWR3157.1

Buehner, M., Houtekamer, P. L., Charette, C., Mitchell, H. L., & He, B. (2010b). Intercomparison of Variational data assimilation and the ensemble Kalman filter for global deterministic NWP. Part II: One-month experiments with real observations. *Monthly Weather Review*, *138*(5), 1567–1586. https://doi.org/10.1175/2009MWR3158.1

Burgers, G., van Leeuwen, P. J., & Evensen, G. (1998). Analysis scheme in the ensemble Kalman filter. *Monthly Weather Review*, *126*(6), 1719–1724. https://doi.org/10.1175/1520-0493(1998)126%3C1719:ASITEK%3E2.0.CO;2

Campbell, W. F., Bishop, C. H., & Hodyss, D. (2010). Vertical covariance localization for satellite radiances in ensemble Kalman filters. *Monthly Weather Review*, *138*(1), 282–290. https://doi.org/10.1175/2009MWR3017.1

Chen, Y., & Oliver, D. S. (2010). Cross-covariances and localization for EnKF in multiphase flow data assimilation. *Computational Geosciences*, *14*(4), 579–601. https://doi.org/10.1007/s10596-009-9174-6

Collard, A. D., & McNally, A. P. (2009). The assimilation of infrared atmospheric sounding interferometer radiances at ECMWF. *Quarterly Journal of the Royal Meteorological Society*, *135*(641), 1044–1058. https://doi.org/10.1002/qj.410

Derber, J. C., & Wu, W.-S. (1998). The use of TOVS cloud-cleared radiances in the NCEP SSI analysis system. *Monthly Weather Review*, *126*(8), 2287–2299. https://doi.org/10.1175/1520-0493(1998)126%3C2287:TUOTCC%3E2.0.CO;2

Emerick, A., & Reynolds, A. (2010). Combining sensitivities and prior information for covariance localization in the ensemble Kalman filter for petroleum reservoir applications. *Computational Geosciences*, *15*, 251–269.

Evensen, G. (1994). Sequential data assimilation with a nonlinear quasi-geostrophic model using Monte Carlo methods to forecast error statistics. *Journal of Geophysical Research*, *99*(C5), 10,143–10,162. https://doi.org/10.1029/94JC00572

Fertig, E. J., Hunt, B. R., Ott, E., & Szunyogh, I. (2007). Assimilating non-local observations with a local ensemble Kalman filter. *Tellus*, *59A*, 719–730.

Gaspari, G., & Cohn, S. E. (1999). Construction of correlation functions in two and three dimensions. *Quarterly Journal of the Royal Meteorological Society*, *125*(554), 723–757. https://doi.org/10.1002/qj.49712555417

Hamill, T. M., Whitaker, J. S., & Snyder, C. (2001). Distance-dependent filtering of background-error covariance estimates in an ensemble Kalman filter. *Monthly Weather Review*, *129*(11), 2776–2790. https://doi.org/10.1175/1520-0493(2001)129%3C2776:DDFOBE%3E2.0.CO;2

Han, Y., Weng, F., Liu, Q., & van Delst, P. (2007). A fast radiative transfer model for SSMIS upper atmosphere sounding channels. *Journal of Geophysical Research*, *112*, D11121. https://doi.org/10.1029/2006JD008208

Houtekamer, P. L., Deng, X., Mitchell, H. L., Baek, S., & Gagnon, N. (2014). Higher resolution in an operational ensemble Kalman filter. *Monthly Weather Review*, *142*(3), 1143–1162. https://doi.org/10.1175/MWR-D-13-00138.1

Houtekamer, P. L., & Mitchell, H. L. (1998). Data assimilation using an ensemble Kalman filter technique. *Monthly Weather Review*, *126*(3), 796–811. https://doi.org/10.1175/1520-0493(1998)126%3C0796:DAUAEK%3E2.0.CO;2

Houtekamer, P. L., & Mitchell, H. L. (2001). A sequential ensemble Kalman filter for atmospheric data assimilation. *Monthly Weather Review*, *129*(1), 123–137. https://doi.org/10.1175/1520-0493(2001)129%3C0123:ASEKFF%3E2.0.CO;2

Houtekamer, P. L., & Mitchell, H. L. (2005). Ensemble Kalman filtering. *Quarterly Journal of the Royal Meteorological Society*, *131*(613), 3269–3289. https://doi.org/10.1256/qj.05.135

Houtekamer, P. L., Mitchell, H. L., Pellerin, G., Buehner, M., Charron, M. and co-authors (2005). Atmospheric data assimilation with the ensemble Kalman filter: Results with real observations. *Monthly Weather Review 133*, 604–620, 3. https://doi.org/10.1175/MWR-2864.1

Hunt, B. R., Kostelich, E. J., & Szunyogh, I. (2007). Efficient data assimilation for spatiotemporal chaos: A local ensemble transform Kalman filter. *Physica D*, *230*(1-2), 112–126. https://doi.org/10.1016/j.physd.2006.11.008

Kang, J.-S., Kalnay, E., Liu, J., Fung, I., Miyoshi, T., & Ide, K. (2011). "Variable localization" in an ensemble Kalman filter. Application to the carbon cycle data assimilation. *Journal of Geophysical Research*, *116*, D09110. https://doi.org/10.1029/2010JD014673

Kazumori, M. (2014). Satellite radiance assimilation in the JMA operational mesoscale 4DVAR system. *Monthly Weather Review*, *142*(3), 1361–1381. https://doi.org/10.1175/MWR-D-13-00135.1

Kleist, D. T., & Ide, K. (2015). An OSSE-based evaluation of hybrid variational-ensemble data assimilation for the NCEP GFS. Part II: 4DEnVAR and hybrid variants. *Monthly Weather Review*, *143*(2), 452–470. https://doi.org/10.1175/MWR-D-13-00350.1

Kleist, D. T., Parrish, D. F., Derber, J. C., Treadon, R., Wu, W., & Lord, S. (2009). Introduction of the GSI into NCEP Global Data Assimilation System. *Weather and Forecasting*, *24*(6), 1691–1705. https://doi.org/10.1175/2009WAF2222201.1

Le Marshall, J., Jung, J., Derber, J., Chahine, M., Treadon, R., Lord, S. J., et al. (2006). Improving global analysis and forecasting with AIRS. *Bulletin of the American Meteorological Society*, *87*(7) 891–895. https://doi.org/10.1175/BAMS-87-7-891

Lei, L., & Anderson, J. L. (2014a). Comparisons of empirical localization techniques for serial ensemble Kalman filters in a simple atmospheric general circulation model. *Monthly Weather Review*, *142*(2), 739–754. https://doi.org/10.1175/MWR-D-13-00152.1

Lei, L., & Anderson, J. L. (2014b). Empirical localization of observations for serial ensemble Kalman filter data assimilation in an atmospheric general circulation model. *Monthly Weather Review*, *142*(5), 1835–1851. https://doi.org/10.1175/MWR-D-13-00288.1

Lei, L., & Anderson, J. L. (2014c). Impacts of frequent assimilation of surface pressure observations on atmospheric analyses. *Monthly Weather Review*, *142*(12), 4477–4483. https://doi.org/10.1175/MWR-D-14-00097.1

Lei, L., Anderson, J. L., & Romine, G. S. (2015). Empirical localization functions for ensemble Kalman filter data assimilation in regions with and without precipitation. *Monthly Weather Review*, *143*(9), 3664–3679. https://doi.org/10.1175/MWR-D-14-00415.1

Lei, L., Anderson, J. L., & Whitaker, J. S. (2016). Localizing the impact of satellite radiance observations using a global group ensemble filter. *Journal of Advances in Modeling Earth Systems*, *8*(2), 719–734. https://doi.org/10.1002/2016MS0000627

Lei, L., & Whitaker, J. S. (2015). Model space localization is not always better than observation space localization for assimilation of satellite radiances. *Monthly Weather Review*, *143*(10), 3948–3955. https://doi.org/10.1175/MWR-D-14-00413.1

Lei, L., & Whitaker, J. S. (2016). A four-dimensional incremental analysis update for the ensemble Kalman filter. *Monthly Weather Review*, *144*, 2605–2621. https://doi.org/10.1175/MWR-D-15-0246.1

Lei, L., Whitaker, J. S., & Bishop, C. H. (2018). Improving assimilation of radiance observations by implementing model space localization in an ensemble Kalman filter. *Journal of Advances in Modeling Earth Systems*, *10*, 3221–3232. https://doi.org/10.1029/2018MS001468

McCarty, W., Jedloveck, G., & Miller, T. L. (2009). Impact of the assimilation of Atmospheric Infrared Sounder radiance measurements on short-term weather forecasts. *Journal of Geophysical Research*, *114*, D18122. https://doi.org/10.1029/2008JD011626

McNally, A. P., Watts, P. D., Smith, J. A., Engelen, R., Kelly, G. A., Thepaut, J. N., & Matricardi, M. (2006). The assimilation of AIRS radiance data at ECMWF. *Quarterly Journal of the Royal Meteorological Society*, *132*(616), 935–957. https://doi.org/10.1256/qj.04.171

Miyoshi, T., & Sato, Y. (2007). Assimilating satellite radiances with a local ensemble transform Kalman filter (LETKF) applied to the JMA global model (GSM). *SOLA*, *3*, 37–40. https://doi.org/10.2151/sola.2007-010

Miyoshi, T., Sato, Y., & Kadowaki, T. (2010). Ensemble Kalman filter and 4D-Var intercomparison with the Japanese Operational Global Analysis and Prediction System. *Monthly Weather Review*, *138*(7), 2846–2866. https://doi.org/10.1175/2010MWR3209.1

Miyoshi, T., Yamane, S., & Enomoto, T. (2007). Localizing the error covariance by physical distance within a local ensemble transform Kalman filter (LETKF). *Scientific Online Letters on the Atmosphere*, *3*, 89–92.

Ott, E., Hunt, B. R., Szunyogh, I., Zimin, A. V., Kostelich, E. J., Corazza, M., et al. (2004). A local ensemble Kalman filter for atmospheric data assimilation. *Tellus*, *56A*, 415–428.

Palmer, T. N., Buizza, R., Doblas-Reyes, F., Jung, T., Leutbecher, M., Shutts, G. J., et al. (2009). Stochastic parameterization and model uncertainty. ECMWF Tech. Memo. 598, 44 pp. [available online at http://www.ecmwf.int/sites/default/files/elibrary/2009/11577-stochastic-parametrization-and-model-uncertainty.pdf].

Snyder, C., & Zhang, F. (2003). Assimilation of simulated Doppler radar observations with an ensemble Kalman filter. *Monthly Weather Review*, *131*(8), 1663–1677. https://doi.org/10.1175//2555.1

Tong, M., & Xue, M. (2005). Ensemble Kalman filter assimilation of Doppler radar data with a compressible nonhydrostatic model: OSS experiments. *Monthly Weather Review*, *133*(7), 1789–1807. https://doi.org/10.1175/MWR2898.1

Wang, C., Lei, L., Tan, Z.-M., & Chu, K. (2020). Adaptive localization for tropical cyclones with satellite radiances in an ensemble Kalman filter. *Frontiers in Earth Science*, *8*. https://doi.org/10.3389/feart.2020.00039

Wang, X., Barker, D., Snyder, C., & Hamill, T. M. (2008). A hybrid ETKF-3DVAR data assimilation scheme for the WRF model. Part I: Observing system simulation experiment. *Monthly Weather Review*, *136*(12), 5116–5131. https://doi.org/10.1175/2008MWR2444.1

Weng, F. (2007). Advances in radiative transfer modeling in support of satellite data assimilation. *Journal of the Atmospheric Sciences*, *64*(11), 3799–3807. https://doi.org/10.1175/2007JAS2112.1

Whitaker, J. S., & Hamill, T. M. (2012). Evaluating methods to account for system errors in ensemble data assimilation. *Monthly Weather Review*, *140*(9), 3078–3089. https://doi.org/10.1175/MWR-D-11-00276.1

Whitaker, J. S., Hamill, T. M., Wei, X., Song, Y., & Toth, Z. (2008). Ensemble data assimilation with the NCEP Global Forecast System. *Monthly Weather Review*, *136*(2), 463–482. https://doi.org/10.1175/2007MWR2018.1

Wu, W. S., Purser, R. J., & Parrish, D. F. (2002). Three-dimensional variational analysis with spatially inhomogeneous covariances. *Monthly Weather Review*, *130*(12), 2905–2916. https://doi.org/10.1175/1520-0493(2002)130%3C2905:TDVAWS%3E2.0.CO;2

Zhen, Y., & Zhang, F. (2014). A probabilistic approach to adaptive covariance localization for serial ensemble square-root filters. *Monthly Weather Review*, *142*(12), 4499–4518. https://doi.org/10.1175/MWR-D-13-00390.1

Zhou, Y., McLaughlin, D., Entekhabi, D., & Ng, G. C. (2008). An ensemble multiscale filter for large nonlinear data assimilation problems. *Monthly Weather Review*, *136*(2), 678–698. https://doi.org/10.1175/2007MWR2064.1